# 博士論文

Functional microzones during sensorimotor activities in relation to aldolase C/zebrin II compartments in mouse cerebellar cortex.

（Aldolase C/zebrin II コンパートメントと運動・知覚機能を司るマウス小脳皮質微小帯域との密接な関連）

堤　新一郎

Shinichiro Tsutsumi

**TABLE OF CONTENTS**

ABSTRACT----------2

INTRODUCTION----------3

MATERIALS AND METHODS----------6

RESULTS----------16

DISCUSSION----------41

ACKNOWLEDGEMENTS----------51

REFERENCES----------52

**ABSTRACT**

Simple and regular anatomical structure is a hallmark of the cerebellar cortex. Parasagittally-arrayed alternate expression of aldolase C/zebrin II in Purkinje cells (PCs) has been extensively studied, but surprisingly little is known about its functional significance. Here I found a precise structure-function relationship between aldolase C expression and synchrony of PC complex spike activities that reflect climbing fiber inputs to PCs. I performed two-photon calcium imaging in knock-in mice in which aldolase C compartments can be visualized *in vivo*, and identified highly synchronous complex spike activities among aldolase C-positive or -negative PCs, but not across these populations. The boundary of aldolase C compartments corresponded to that of complex spike synchrony at single cell resolution. Sensory stimulation evoked aldolase C compartment-specific complex spike responses and synchrony. This result further revealed the structure-function segregation. In awake animals, complex spike synchrony both within and between PC populations across the aldolase C boundary were enhanced in response to sensory stimuli, in a way that two functionally distinct PC ensembles are co-activated. These results suggest that PC populations characterized by aldolase C expression precisely represent distinct functional units of the cerebellar cortex, and these functional units can cooperate to process sensory information in awake animals.

## INTRODUCTION

The cerebellar cortex has an elaborate parasagittal organization that consists of several longitudinal ‘zones’ [1]. The zones were originally defined by their topographically organized Purkinje cell (PC) output to distinct subdivision within the cerebellar nuclei [2]. Both anatomical and physiological studies have shown that the zones receive climbing fiber projections from the individual inferior olivary subnuclei [1, 3]. Some of the zones were further subdivided into longitudinal ‘microzones’ using high-resolution electrophysiological olivo-cerebellar mapping [3]. Therefore, the zones are hypothesized to control particular motor mechanisms and the microzones control different aspects of motor function within the mechanisms, thus represent functional units in the cerebellar cortex [4, 5].

Neighboring PCs located within the zones tend to show synchronous complex spike activities [6, 7]. Synchronous complex spike activities in the rostro-caudal direction are thought to arise from rostro-caudal projection of single climbing fibers [8, 9]. The complex spike synchrony in the medio-lateral direction is thought to be caused by gap junctional electrical couplings between inferior olivary neurons [10]. Recent two-photon imaging studies have revealed spatially fine longitudinal structures with high complex spike synchrony in the medio-lateral direction [11-14]. PCs within these

structures are synchronized spontaneously or by sensorimotor inputs, thus surely receive similar climbing fiber inputs. Therefore, these fine scale synchronous structures are thought to represent the microzones [11, 13].

The cerebellar cortex is also divided into longitudinal stripes by the molecular expression in PCs [15-19]. Among the molecules that show longitudinal expression patterns, aldolase C/zebrin II and its expression have been extensively studied because of its excellence as a marker. Seven aldolase C-positive (1+ to 7+) and -negative (1- to 7-) compartments are known to exist in each hemicerebellum [15]. These aldolase C compartments are shown to extensively co-localize with the longitudinal zones [9]. A previous study has addressed the relationships between the zones and complex spike synchrony using multi-electrodes and found that complex spikes tend to synchronize within the aldolase C compartments [20]. However, no study has addressed the cell-level precise relationships between the anatomically defined zones and the functionally defined microzones, in which complex spikes are highly synchronized.

To elucidate the structure-function relationships between the zones represented by aldolase C expression and fine scale complex spike synchrony in the medio-lateral direction, I visualized aldolase C compartments *in vivo* using a novel knock-in mouse line (Aldoc-tdTomato) and performed two-photon calcium imaging. I found that

spontaneous complex spike synchrony was tightly regulated to be within the aldolase C compartments at single cell resolution. The synchrony was not homogenous within the compartment but attenuated in the medio-lateral direction, and multiple synchronous structures existed within the zones. I identified a microzone which responds to perioral air puff stimulation. The boundary of the microzone corresponded to that of aldolase C expression. During the stimulation, synchronous complex spike activities were induced within the microzone. I also found that distinct microzones located within different aldolase C compartments were co-activated in awake mice. Together, the aldolase C compartments are shown to be separated into several functional microzones, in which complex spikes are highly synchronized either spontaneously or by sensory inputs. The functional microzones across different zones can be co-activated during sensorimotor activities.

## MATERIALS AND METHODS

### Animals

All experiments were performed according to national guidelines and were approved by the Animal Experiment Committees of The University of Tokyo, Niigata University, and Hokkaido University. The Aldoc-tdTomato knock-in mice were produced by homologous recombination in RENKA C57BL/6N-derived embryonic stem cells [21]. The targeting vector was designed with a tdTomato protein sequence followed by a neomycin resistance cassette (Neo) inserted in frame just behind the translational initiation site of the aldolase C gene (Aldoc) (Fig. 1A). This targeting vector was constructed with a 12 kb C57BL/6 genomic fragment (6.4 kb upstream and 5.57 kb downstream of the translational initiation site) and diphtheria toxin gene (DT) using a BAC subcloning kit (Gene Bridges, Dresden, Germany). ES cell clones with the correct recombination were identified by Southern blotting using the 5'-probe on EcoR V-digested genomic DNA and the 3'-probe on Sac I-digested genomic DNA. Chimeric mice were generated as described previously [5]. Heterozygous mice ($Aldoc^{tdTomato/+}$) were used for further analysis. No overt phenotype was detected in heterozygous mice, as described previously [22].

**Immunohistochemistry**

Under deep pentobarbital anesthesia, Aldoc-tdTomato mice were transcardially perfused with 4% paraformaldehyde in 0.1 M sodium phosphate buffer. Coronal microslicer sections were then processed (50 μm in thickness; VT1000S; Leica). For immunofluorescence, the sections were successively incubated in a free floating state at room temperature with 10% normal donkey serum for 20 minutes, goat calbindin antibody (a marker of PCs) and a rabbit anti-aldolase C antibody, and Alexa 488- and Cy5-conjugated species-specific secondary antibodies (1:200, Invitrogen; Jackson ImmunoResearch) for 2 hr. Images were taken with a confocal laser scanning microscope (FV1000; Olympus) equipped with a helium-neon/argon laser and a PlanApo (10×/0.40) and a PlanApoN (60×/1.42, oil immersion) objective lens.

**Animal preparation and *in vivo* two-photon imaging**

Adult heterozygous Aldoc-tdTomato mice (postnatal days > 60) of both sexes were used for all the experiments. They showed no overt phenotype like ataxia or motor dysfunction. The mice were anesthetized with ketamine/xylazine (100/10 mg/kg). I chose this anesthesia for calcium imaging because of the ease in experimental preparation (e.g. easier to control bleeding and less brain swelling compared to

isoflurane anesthesia). Animals were put on a warm blanket and body temperature was kept at 37°C. The depth of anesthesia was constantly monitored by observing forelimb pinch withdrawal reflexes, and additional injections of anesthetics were given as needed. The skin and muscles above the cerebellum were removed and a custom-made metal plate was fixed with superglue and dental acrylic cement. A ~2 mm craniotomy was performed over the left or right folium Crus IIa (4 mm lateral and 2 mm posterior to the occipital bone line) and the dura mater was carefully removed. Agarose (1.5%) and a glass coverslip were mounted over the craniotomy to reduce motion artifacts due to respiration and heartbeat.

All the imaging experiments were performed using a custom-built two-photon microscope (Sutter Instruments) with 40× objective lens (Olympus) controlled with ScanImage software [23] for Matlab (MathWorks). Two-photon excitation was achieved with a pulsed Ti:Sapphire laser (wavelength of 830 nm for OGB-1 AM calcium imaging, 800 nm for Cal-520 calcium imaging, 950 nm for RFP imaging, 80 MHz repetition rate, and 100 fsec pulse width; Mai Tai, Spectra-Physics). Average laser power was adjusted to be less than 20 mW (typically 5-10 mW for calcium imaging, and 7-12 mW for tdTomato imaging) to avoid phototoxicity. Fluorescence signals were divided into green and red channels with a dichroic mirror and emission filters (Chroma), and detected

with a pair of photomultiplier tubes (Hamamatsu).

I first imaged tdTomato fluorescence to identify the boundary of aldolase C compartments. Compartmental expression of tdTomato in PCs was easily visualized by two-photon microscopy (Fig. 1B). The characteristic width and sequence of mouse aldolase C compartments in Crus II [19] aided the identification and naming of each compartment. The entire location of all the compartments in the imaging field was manually mapped in advance because I later injected a red fluorescent dye, Alexa 594, which would blur the boundaries. A high resolution 3D stack (512 × 512 pixels, 220 μm each, and 3 μm per slice) was acquired from the pial surface to the PC soma on the aldolase C compartment boundary. This image stack was used as a reference for calcium imaging.

An AM ester calcium indicator dye (Oregon Green 488 BAPTA-1 AM, (OGB-1 AM), Invitrogen, or Cal-520 AM, AAT Bioquest) was bulk-loaded using a protocol as described previously [24, 25]. Briefly, OGB-1 AM or Cal-520 AM (~200 μM) was dissolved in DMSO with 10% w/v Pluronic F-127 (Invitrogen). The aliquot of dye was mixed with Alexa 594 fluorescent dye (20 μM; Invitrogen) and placed into a glass pipette (4 MΩ). The dye solution was injected into the cerebellar molecular layer. Two injections were performed at 15-20 psi for 5 minutes using a Picospritzer (General

Valve). Successful dye ejection was monitored through the Alexa channel on two-photon imaging. 1-3 hours after dye loading, calcium imaging was performed on the aldolase C compartment boundaries. The locations of the boundaries were roughly identified by using an aldolase C map obtained prior to dye injection. The pattern of blood vessels was compared to that present in the tdTomato images to precisely adjust the boundary locations. To obtain calcium transients from the PC dendrites, horizontal full frame scan movies were acquired at 128 × 128 pixels resolution, and 1000 frames at 7.8 Hz. In a subset of the calcium imaging experiments, timed air puff stimuli (40-45 psi for 50 ms, every 10 seconds, 13 times in 128 seconds) were applied at the ipsilateral perioral surface using a Picospritzer.

**Pharmacology**

In a subset of calcium imaging experiments, carbenoxolone (120 mg/kg, Sigma) or harmaline (1 mg/kg, Sigma) was intraperitoneally injected during anesthesia. At first, baseline calcium imaging was performed before the drug injection. Subsequent imaging was performed 30 minutes after the injection.

**Imaging in awake mice**

To perform imaging in awake mice, they were acclimated to the head fixation for ~30 min prior to imaging. After imaging under anesthesia, mice were allowed to recover from anesthesia and then imaging was performed during the awake state. Vigilance state was determined by monitoring sporadic active movements, e.g., whisking, grooming, eye blink or limb and body movements. I determined that mice were awake if they were actively whisking and exhibited reflex body movements in response to the air puff stimuli.

**Electrophysiology**

Adult heterozygous Aldoc-tdTomato mouse (postnatal days > 60) was anesthetized with isoflurane (1.0-1.5%). A shadowpatching technique [26] was utilized for *in vivo* cell-attached recordings from PCs. A glass electrode filled with extracellular solution containing Alexa dye (5 MΩ) was navigated through the two-photon microscope and targeted at the PC soma. About 5 minutes after the establishment of loose-seal, a current-clamp recording was performed for 2 minutes during simultaneous dendritic calcium imaging. Data were obtained using a MultiClamp 700B amplifier (Molecular Devices), filtered at 10 kHz and digitized at 20 kHz using a Digidata 1322A (Axon instruments) controlled by AxoGraph X software (AxoGraph Scientific).

**Data analysis**

For the analysis of calcium imaging data, regions of interest (ROIs) corresponding to the active PC dendrites were detected using custom-made Matlab routines (Matlab R2013a, MathWorks). I totally automated a previously described correlation-based detection method [11, 27, 28] and succeeded in minimizing the time required for human supervision (typically 1-2 minutes for each dataset). For all the analyses, a correlation coefficient was calculated using the following equation;

$$C_{ij(\tau)} = \frac{\sum_{t=0}^{T} X_{i(t)} X_{j(t+\tau)}}{\sqrt{\sum_{t=0}^{T} \{X_{i(t)}\}^2 \sum_{t=0}^{T} \{X_{j(t)}\}^2}}$$

where $X_i$ and $X_j$ are fluorescent traces of ith and jth pixels or dendrites, T is total recording time, and $\tau$ is lag time between the two traces. $C_{ij}$ (0), cross-correlation coefficient at zero lag time, was defined as synchrony.

To extract the fluorescence changes corresponding to the calcium transients, the raw movie was first converted to $\Delta F/F$ wave, expressed as $\Delta F/F = (F-F_0) / (F_0-F_b)$, where $F_0$ is the baseline fluorescence in the absence of calcium transients and $F_b$ is the background fluorescence. $F_0$ was defined as follows. First, I calculated a threshold as

mean + 1SD of the F wave of each pixel, and then the F wave below the threshold was averaged to obtain $F_0$. The minimum fluorescence of the stack was assigned to $F_b$, which usually corresponded to the pixel located within a blood vessel. The ΔF/F wave of each pixel was then high-pass filtered at 0.1 Hz to eliminate slow drifts presumably due to photo-bleaching effects or glial signals.

As PC dendrites elongate almost parallel to each other in a sagittal plane, I calculated the direction of the dendrites to aid auto-detection of ROIs. The imaging field was segmented into sets of 4 pixel width strips, 0 degree to 45 degrees from the vertical line. Correlation coefficients between the mean ΔF/F wave of each strip and that of each pixel within the strip were calculated and summed. The values calculated in certain sets of strips were further summed. The angle of the strip set with a maximal correlation value was the detected PC dendritic angle (Fig. 3Bb).

The imaging field was again segmented into 6 pixel width (10.3 μm) strips in the direction of the calculated angle. A summed correlation coefficient between the ΔF/F waves from all the pixels within a strip was plotted (Fig. 3Bc). Seed pixels (3 to 30) with the highest correlation value were recorded, and the mean correlation coefficient between the ΔF/F wave of seed pixels and that of all the pixels were plotted on each pixel. This procedure highlighted the shape of PC dendrites (Fig. 3Bd). Images were

then filtered and binarized using an adaptive threshold filter (adaptive threshold, available online at Matlab central; window size: 256, constant: 0.1). ROIs were selected from the binarized image (Fig. 3Be). Averaged ΔF/F waves within detected ROIs were calculated and apparent false positives (e.g. no calcium signals at all) were manually omitted to yield the final set of ROIs (Fig. 3Bf).

For experiments with sensory stimulation, I defined responsive dendrites at a given trial as those satisfying the following two criteria. 1) Calcium transient peaks were observed between 0-128 ms after the onset of the air puff. This is because it takes 128 ms to acquire one frame and true complex spike responses should be less than 128 ms in duration. 2) The peak exceeds the mean + 2 SD from the baseline, which was calculated from ΔF/F waves 0 to 1 second before the onset of the air puff. Response probability for one dendrite was calculated from one imaging session (13 trials). The response probabilities of all the dendrites from all the mice were averaged in reference to the aldolase C boundaries (Fig. 5D). The synchrony of sensory-evoked responses was calculated using ΔF/F waves 0 to 2 seconds after the onset of air puff (Fig. 6E, top row). Spontaneous synchrony was calculated for the same time period in the absence of air puff stimulation (Fig. 6E, middle row).

Electrophysiological data analysis was performed using Igor Pro software

(WaveMetrics). All statistical analyses were performed using R ver. 3.0.0 (http://www.r-project.org/).

## RESULTS

### Visualization of aldolase C compartments *in vivo*

To visualize aldolase C-expressing PCs in intact mice, I used a targeted knock-in approach to generate Aldoc-tdTomato mouse line. In the cerebellum of these mice, red fluorescent protein, tdTomato, was expressed under the control of aldolase C gene (*Aldoc*) promoter (Fig. 1A). Recently, a similar strategy was employed to visualize aldolase C expression using Aldoc-Venus knock-in mice [22]. Two-photon imaging of the cerebellar cortex in Aldoc-tdTomato mice revealed that the boundaries of aldolase C expression across the molecular layer to the PC layer were clear at single cell resolution (Fig. 1B). To check whether the red fluorescence of tdTomato correctly reflected aldolase C expression and whether knock-in affects the aldolase C expression pattern, I immunolabeled cerebellar sections of Aldoc-tdTomato mice with both anti-calbindin and anti-aldolase C antibodies. As a result, aldolase C expression pattern in Aldoc-tdTomato mice was the same as that in wild type animals (Fig. 1Ca4) [19]. In Aldoc-tdTomato mice, tdTomato fluorescence was specifically and exclusively observed in PCs expressing aldolase C in both the whole cerebellar cortex (Fig. 1Ca) and the folium Crus II (Fig. 1Cb-c).

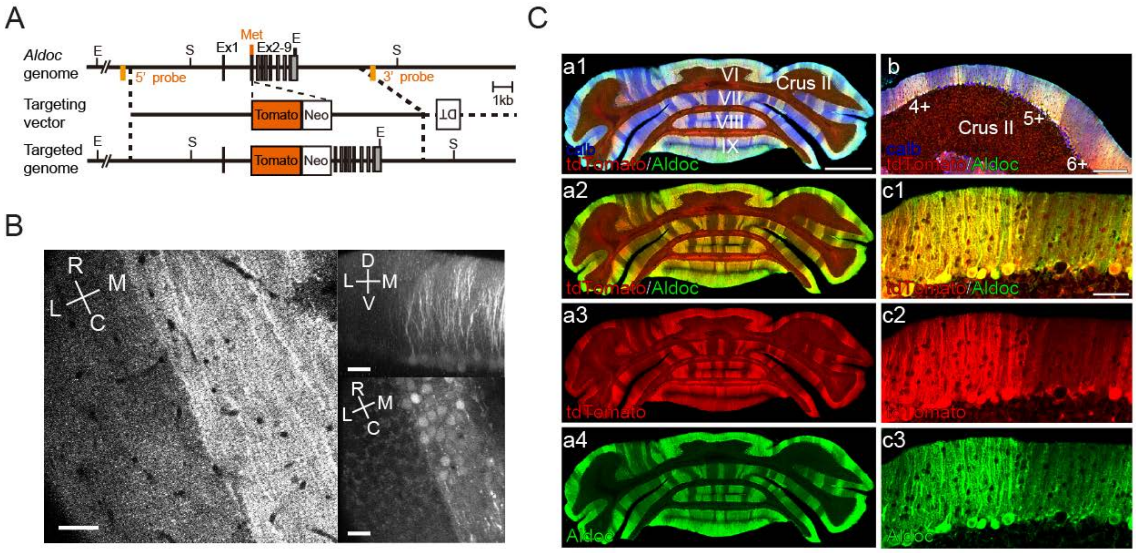


**Figure 1.**

Aldolase C expressions in single PCs are visualized *in vivo*.

***A***, Knock-in construct of Aldoc-tdTomato mouse line. Gray boxes indicate exon 1-9. Met: initial methionine, DT: diphtheria toxin gene, Tomato: tdTomato coding sequence followed by a polyA addition signal sequence, Neo: pgk-gb2 neomycin resistance cassette, E: EcoR V, S: Sac I. ***B***, Two-photon imaging of aldolase C compartments *in vivo*. A single horizontal plane in the molecular layer (left) and XZ (right top) and XY (right bottom) projection of the image stack. R: rostral, C: caudal, L: lateral, M: medial, D: dorsal, V: ventral. Scale bars: 40 μm. ***C***, A representative coronal section of the cerebellum taken from an Aldoc-tdTomato mouse immunostained with anti-calbindin and anti-aldolase C antibodies. (a1) Calbindin immunostaining (blue), aldolase C immunostaining (green), and tdTomato fluorescence (red) were overlaid. (a2) Aldolase C immunostaining and tdTomato fluorescence. (a3) tdTomato fluorescence only. (a4) Aldolase C immunostaining only. (b) Calbindin immunostaining, aldolase C immunostaining, and tdTomato fluorescence at the left Crus II in which calcium imaging was performed. Expressions at 4+ to 6+ compartments are shown. (c1) tdTomato fluorescence and aldolase C immunostaining at the boundary of aldolase C expression. (c2) tdTomato fluorescence only. (c3) Aldolase C immunostaining only. calb: calbindin immunostaining, tdTomato: tdTomato fluorescence, and Aldoc: aldolase C immunostaining. Scale bars: 1 mm in a, 200 μm in b, and 50 μm in c.

**Basic firing properties are different between aldolase C-positive and -negative PCs**

I next examined whether electrophysiological properties of PCs depend on the aldolase C expression. Loose-seal cell-attached recordings were performed on PCs within aldolase C compartments (5+ to 7+, lateral 5 compartments in folium Crus IIa) under isoflurane anesthesia. I recorded spontaneous simple and complex spike activities of both aldolase C-positive and -negative PCs. As a result, simple spike firing frequency tended to be lower and complex spike firing frequency tended to be higher in the aldolase C-positive PCs, although the differences were not statistically significant (Fig. 2). Complex spike activities were less regular, complex spike-induced simple spike pauses were longer (Fig. 2A and B), and the number of spikelets in each complex spike was smaller in the aldolase C-positive PCs (Fig. 2C).

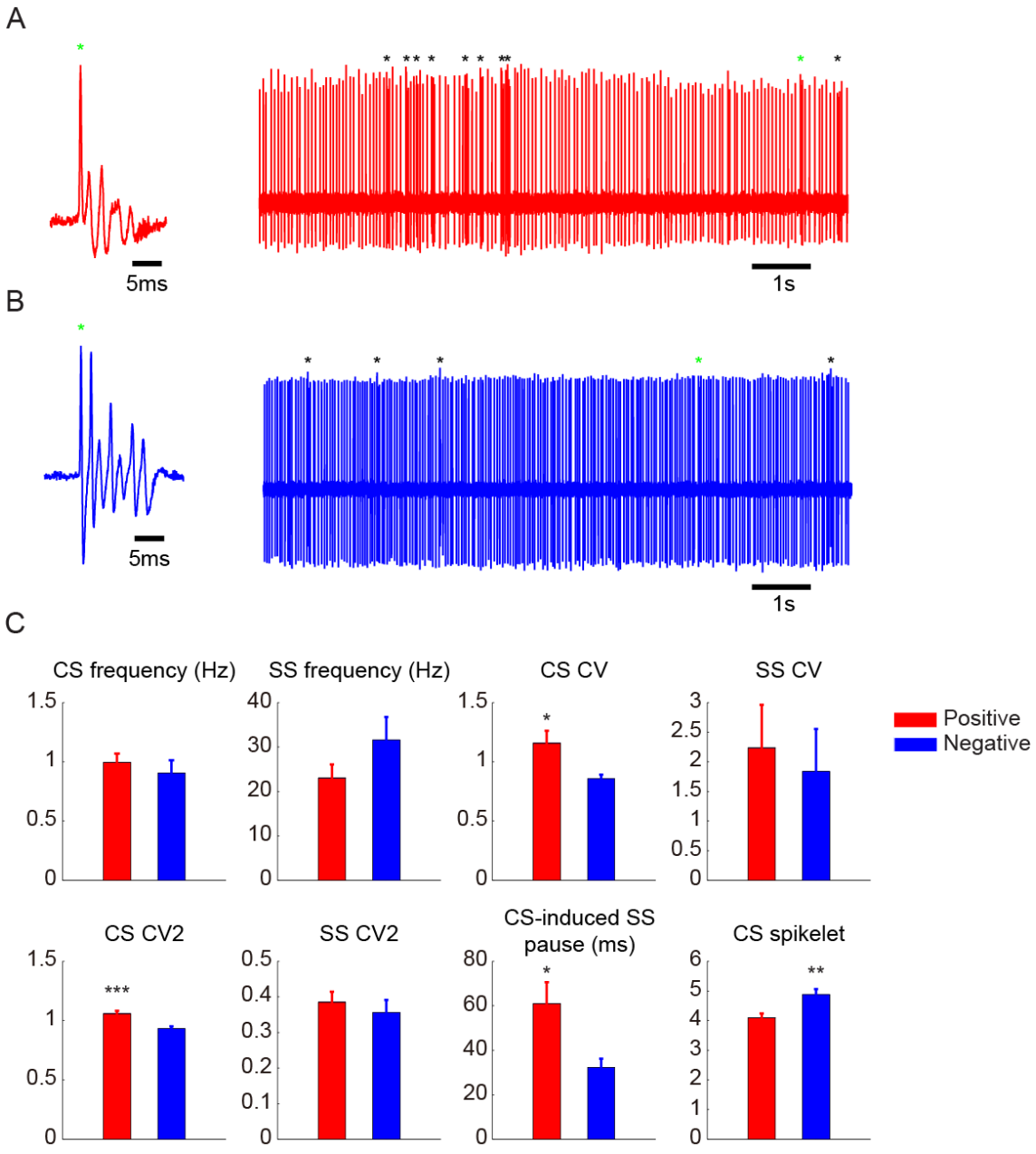


**Figure 2.**

Firing properties of aldolase C-positive and -negative PCs.

***A***, A representative cell-attached recording from an aldolase C-positive (6+) PC. Asterisks represent complex spikes. The complex spike marked with green asterisk is magnified on the left. ***B***, Same as A, but from an aldolase C-negative (5-) PC from the same animal. ***C***, Bar graphs of averaged firing properties of the aldolase C-positive and -negative PCs. Data are represented as mean ± SEM. *n* = 19, 17 cells for aldolase C-positive and -negative compartments, respectively. Red traces and bars represent data

from aldolase C-positive PCs. Blue traces and bars represent data from aldolase C-negative PCs. CS: complex spike, SS: simple spike, CV: coefficient of variation. *: $p < 0.05$, **: $p < 0.01$, ***: $p < 0.001$, Mann Whitney U test.

| | 7+ | 6- | 6+ | 5- | 5+ | positive | negative |
|---|---|---|---|---|---|---|---|
| CS frequency (Hz) | 1.26 | 0.82 | 0.82 | 0.91 | 1.17 | 0.99 ± 0.08 | 0.91 ± 0.11 |
| SS frequency (Hz) | 19.56 | 39.70 | 22.56 | 31.08 | 30.39 | 23.01 ± 3.04 | 31.59 ± 5.14 |
| CS CV | 1.01 | 0.70 | 1.01 | 0.87 | 1.94 | 1.16 ± 0.10* | 0.86 ± 0.03 |
| SS CV | 1.36 | 0.32 | 0.98 | 1.93 | 8.29 | 2.24 ± 0.72 | 1.84 ± 0.71 |
| CS CV2 | 1.02 | 0.96 | 1.10 | 0.93 | 0.96 | 1.06 ± 0.03*** | 0.93 ± 0.02 |
| SS CV2 | 0.49 | 0.31 | 0.36 | 0.36 | 0.30 | 0.39 ± 0.03 | 0.36 ± 0.04 |
| CS-induced SS pause (ms) | 64.50 | 23.35 | 61.60 | 32.90 | 52.45 | 60.92 ± 9.65* | 32.33 ± 3.86 |
| CS spikelets | 4.21 | 4.26 | 4.00 | 4.92 | 4.28 | 4.09 ± 0.14 | 4.88 ± 0.18** |
| | 5 cells | 1 cell | 11 cells | 16 cells | 3 cells | 19 cells | 17 cells |

**Table 1.**

Firing properties of PCs in each aldolase C compartment.

Mean firing properties of PCs in the lateral 5 aldolase C compartments in Crus IIa (5+ to 7+). These data are further averaged for aldolase C-positive and -negative PCs and represented as mean ± SEM (same as Fig. 2C). CS: complex spike, SS: simple spike, CV: coefficient of variation. *: $p < 0.05$, **: $p < 0.01$, ***: $p < 0.001$, Mann Whitney U test.

**Synchronous complex spike activities in the PC populations are sharply delineated at the boundaries of aldolase C expression**

To investigate the relationship between the aldolase C compartmentalization and synchronous complex spike activities at single cell resolution, PCs in the cerebellar folium Crus IIa of Aldoc-tdTomato mice were bulk-loaded with OGB-1 or Cal-520. I chose Crus IIa because it is easy to access and has unique and consistent aldolase C banding with relatively wide compartments (4+ to 7+) [19], which facilitates the analysis of synchrony between PC populations. Spontaneous dendritic calcium transients of PCs, which reflect complex spikes [29] (Fig. 3A), were recorded at the boundaries of aldolase C expression under ketamine/xylazine anesthesia (Fig. 3C and D). I found a significant correlation between complex spike synchrony and the aldolase C expression. Complex spike activities were highly synchronized between aldolase C-positive PCs and between aldolase C-negative PCs (Fig. 3D). However, they were far less synchronized across the aldolase C-positive and -negative PCs. A color-coded correlation matrix clearly showed that the boundary of high synchrony areas precisely corresponded to that of aldolase C expression, determined at single cell resolution (Fig. 3E).

Aldoc-tdTomato mouse line has a great advantage on *in vivo* two-photon

imaging because one can identify the named aldolase C compartments and observe the same set of PCs across different animals. Therefore, I could examine the location dependence of the relationships between the aldolase C compartments and complex spike synchrony. The complex spike synchrony was evaluated around the boundaries of aldolase C compartments from 5a+ to 7+ in Crus IIa (lateral 5 boundaries). I found that boundaries of high complex spike synchrony apparently corresponded to those of aldolase C expression for 7+/6-, 5-/5+, and 5+/5a- (Fig. 4A). In contrast, the boundaries of complex spike synchrony were blurred at 6-/6+ and 6+/5-. These patterns were consistently observed in individual animals (Supplementary Fig. 1) and across corresponding boundaries of left and right lobules (5+/5- boundary; see Fig. 4A fourth panel and Fig. 4D, $n$ = 8 and 6 mice, respectively). Mean synchrony between PC dendrite pairs located less than 100 μm in the mediolateral direction was significantly higher within the aldolase C compartments than across the compartments for overall dataset (Fig. 4B). Post hoc comparison showed significant difference in the 7+/6-, 5-/5+, and 5+/5a- boundaries. This was true for any group of dendritic pairs located with distances less than 80 μm in these representative areas (Fig. 4C). However, synchrony between distant (>100 μm) PC pairs within these compartments were comparable to those across the compartments (Fig. 4C). Moreover, I found more than one high

synchrony areas with clear boundary within single aldolase C compartments (Fig. 4A, 5a- in right most panel and Fig. 4E, right panel). I also found significant attenuation of complex spike synchrony along medio-lateral distance between the same sets of PCs within the aldolase C compartments (Fig. 4C; $p < 0.001$, two way ANOVA).

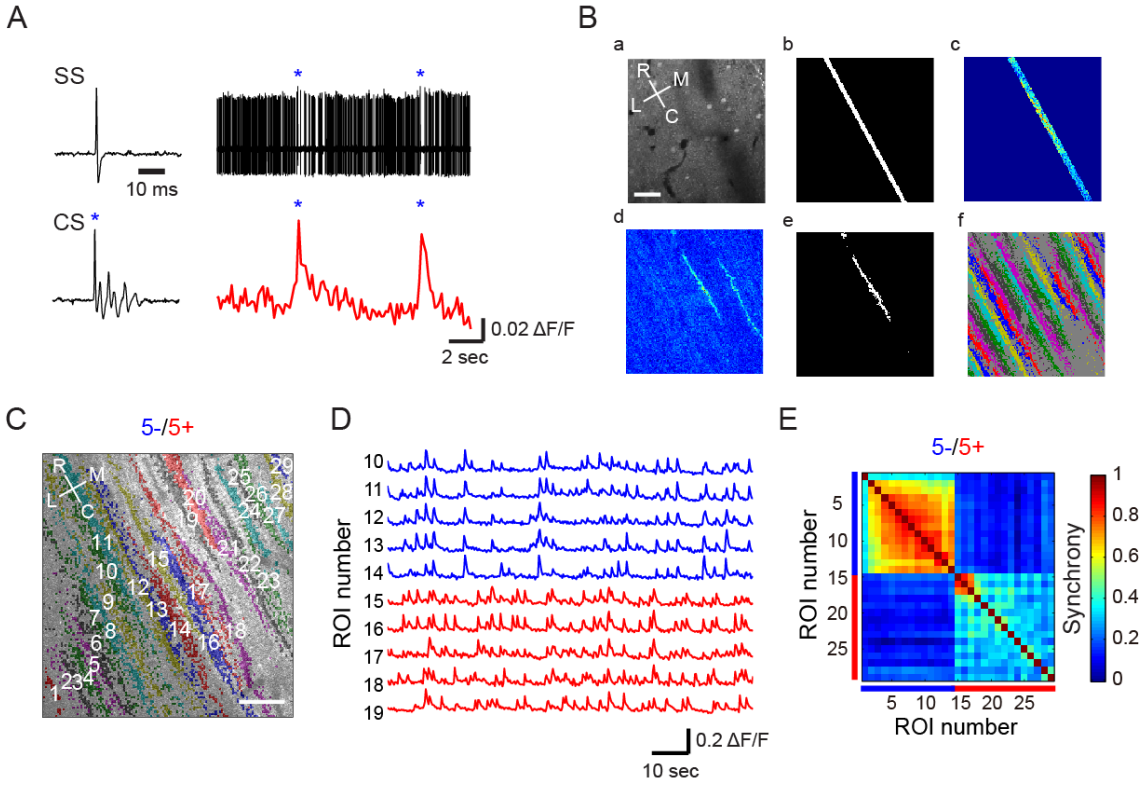


**Figure 3.**

Boundaries of aldolase C expression correspond to those of complex spike synchrony at single cell resolution.

***A***, Left, example waveforms of simple spike and complex spike. Right, simultaneous cell-attached recording (upper) and dendritic calcium imaging (lower) from the same PC. Blue asterisks represent complex spike peaks. SS: simple spike, CS: complex spike. ***B***, (a) An example image from a raw movie of OGB-1 AM calcium imaging. (b) Detected angle of PC dendrites. (c) Color-coded correlation coefficient between a certain pixel and all the pixels in the strip. (d) Color-coded correlation coefficient between seed pixels and all the pixels in the imaging field. (e) Adaptive threshold filtered map from d. Only one region of interest around the seed pixels was selected. (f) Pseudo-colored map of the regions of interest. ***C***, Calcium imaging was performed at a representative aldolase C compartment boundary (5-/5+). Pseudo-colored regions of interest (PC dendrites) are overlaid to the corresponding tdTomato image. ***D***, Representative ΔF/F waves taken from C. Red and blue traces are from aldolase C-positive and -negative PCs, respectively. ***E***, Correlation matrix calculated by using ΔF/F waves from all the dendrite pairs in C. Red and blue bars denote aldolase

C-positive and -negative PCs, respectively. R: rostral, C: caudal, L: lateral, and M: medial. Scale bars: 40 μm.

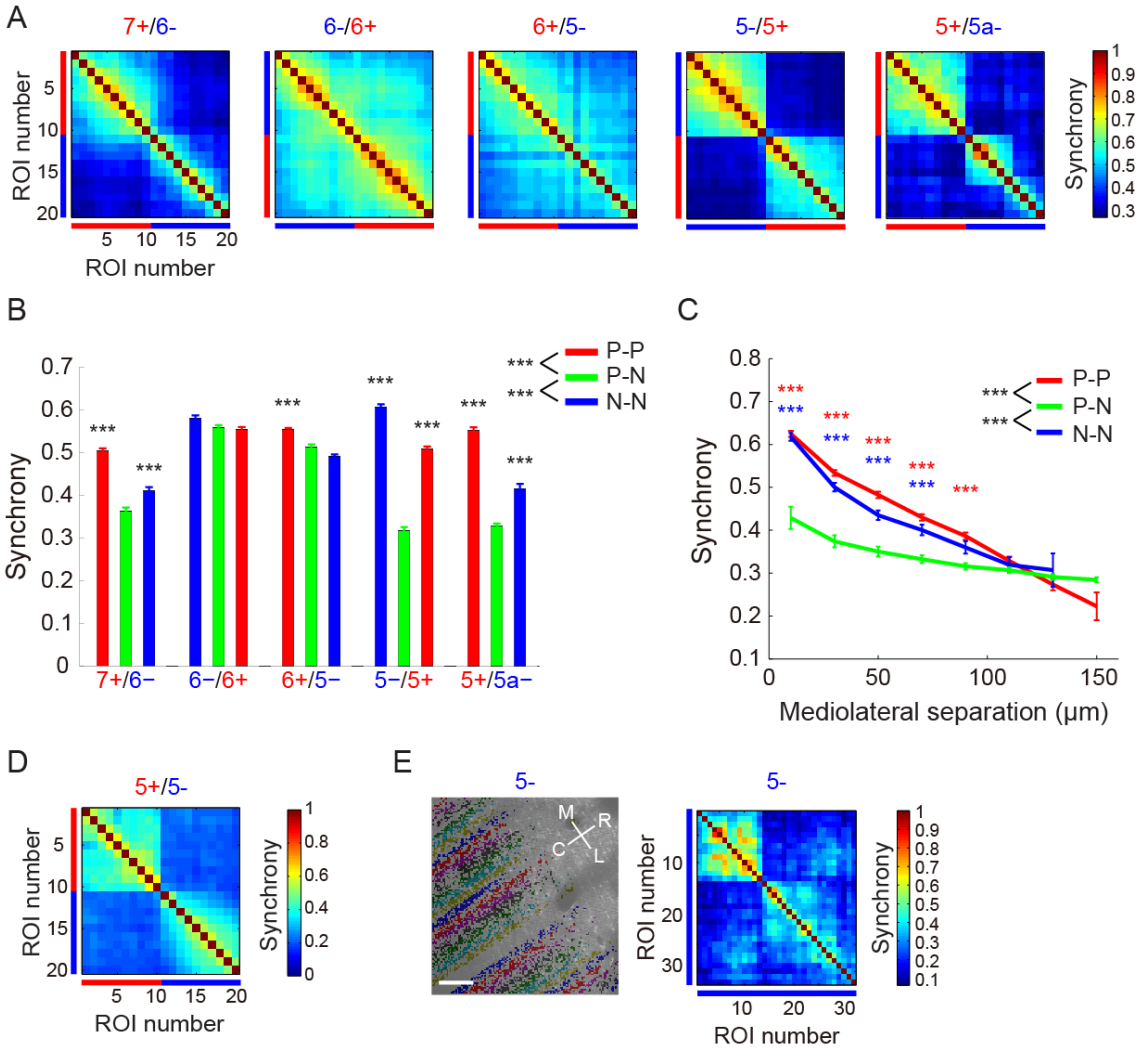


**Figure 4.**

Location dependence of relationships between aldolase C compartments and complex spike synchrony.

***A***, Correlation matrices between ΔF/F waves from 20 adjacent dendrites across aldolase C boundaries; 10 dendrites each from both sides of the boundaries in left Crus II. Data are averaged across mice. Red and blue bars represent aldolase C-positive and -negative PCs, respectively. *n* = 6, 7, 8, 6, and 3 mice for the 7+/6-, 6-/6+, 6+/5-, 5-/5+, and 5+/5a- boundary, respectively. ***B***, Synchrony between ΔF/F waves from PC dendrite pairs whose mediolateral distance less than 100 μm located within and across the aldolase C compartments. Data are represented as mean ± SEM. P-P (red bars): synchrony of ΔF/F waves between the aldolase C-positive PCs, P-N (green bars): that across aldolase C-positive and -negative PCs, and N-N (blue bars): that between the aldolase C-negative PCs. ***: $p < 0.001$, two-way ANOVA followed by post-hoc Tukey

test. ***C***, Calcium transient synchrony plotted against the mediolateral separation between PC dendrite pairs. Data from 7+/6-, 5-/5+, and 5+/5a- boundaries are averaged (4670 dendrite pairs, *n* = 12 mice). P-P (red trace), P-N (green trace), and N-N (blue trace) represent synchrony between aldolase C-positive to -positive, -positive to -negative, and -negative to -negative PC dendrite pairs, respectively. Data are averaged within 20 μm bin and represented as mean ± SEM. Red and blue asterisks denote significant difference between P-P and P-N, N-N and P-N, respectively. ***: $p < 0.001$, two-way ANOVA followed by post-hoc Tukey test. ***D***, Same as A, but only 5+/5- boundary in Crus IIa of right hemisphere. *n* = 6 mice. ***E***, Left, Calcium imaging using Cal-520 was performed within a single aldolase C compartment (5-) in Crus IIa of right hemisphere. Pseudo-colored regions of interest are overlaid to the corresponding tdTomato image. Right, Correlation matrix calculated by using ΔF/F waves from all the dendrite pairs in the corresponding images on the left. Blue bars represent aldolase C-negative PCs. R: rostral, C: caudal, L: lateral, and M: medial. Scale bars: 40 μm.

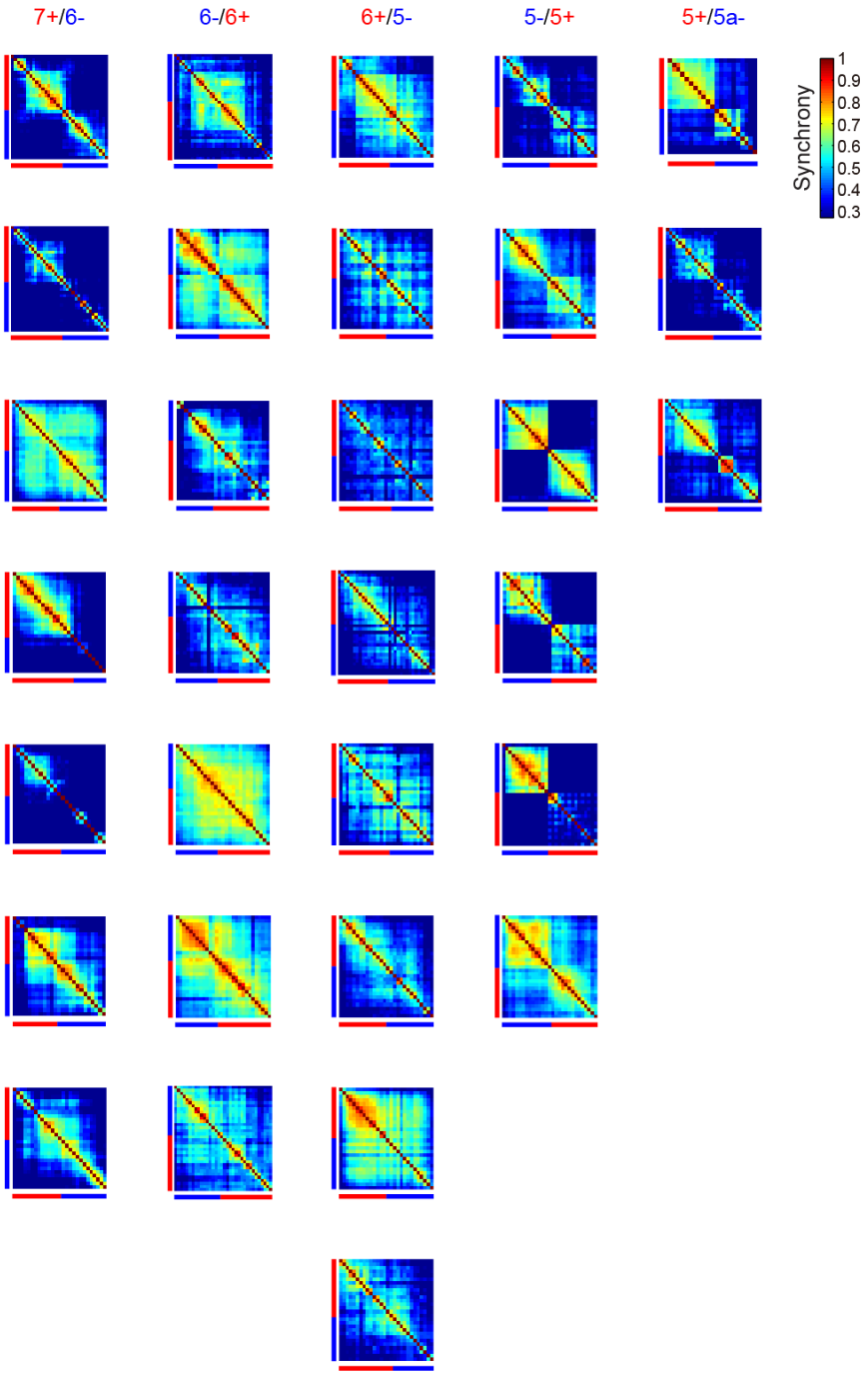


**Supplementary Figure 1.**

Relationships between aldolase C expression and complex spike synchrony are consistent across animals.

Spontaneous correlation matrices from all the imaging sessions. Each column represents data from the boundaries of aldolase C expression indicated on top of the column.

Matrices within each column were obtained from different animals. Red and blue bars represent the aldolase C-positive and -negative PCs, respectively. Note that the pattern of synchrony is fairly consistent across different mice within the same location.

**Neither carbenoxolone nor harmaline influences the structure-function relationship**

Next, I asked why spontaneous complex spike synchrony is finely delineated at some of the boundaries of aldolase C expression. A previous study suggests that gap-junctional electrical couplings between inferior olivary neurons are responsible for the synchronous complex spike firing between closely located PCs [12]. Carbenoxolone is shown to block gap junctions in the inferior olive and reduces coupling between inferior olivary neurons [10, 24]. I therefore examined the effect of carbenoxolone on complex spike synchrony at the boundaries of aldolase C expression. I used the same dose as the previous study where it was effective [24]. However, I did not observe any change in the frequency of dendritic calcium transient (Fig. 5A). The boundary of synchrony in relation to that of aldolase C compartments remained unchanged after carbenoxolone injection (Fig. 5B). Other possible mechanisms for the synchronous complex spike activities in the aldolase C compartments are common inputs to weakly coupled inferior olivary neurons or finely delineated climbing fiber projections from inferior olivary subnuclei to PCs. So I next examined the former mechanism using harmaline, which enhances rhythm-generating ionic current of inferior olivary neurons [30], thus increases input-independent firing of these neurons. I found that frequency of dendritic

calcium transient was significantly increased in both aldolase C-positive and -negative PCs after harmaline application (Fig. 5C). However, the boundary of complex spike synchrony remained unchanged (Fig. 5D). These results suggest that the boundaries of complex spike synchrony at those of aldolase C expression are largely maintained by finely delineated climbing fiber projections from individual inferior olivary subnuclei to PCs in the corresponding aldolase C compartments.

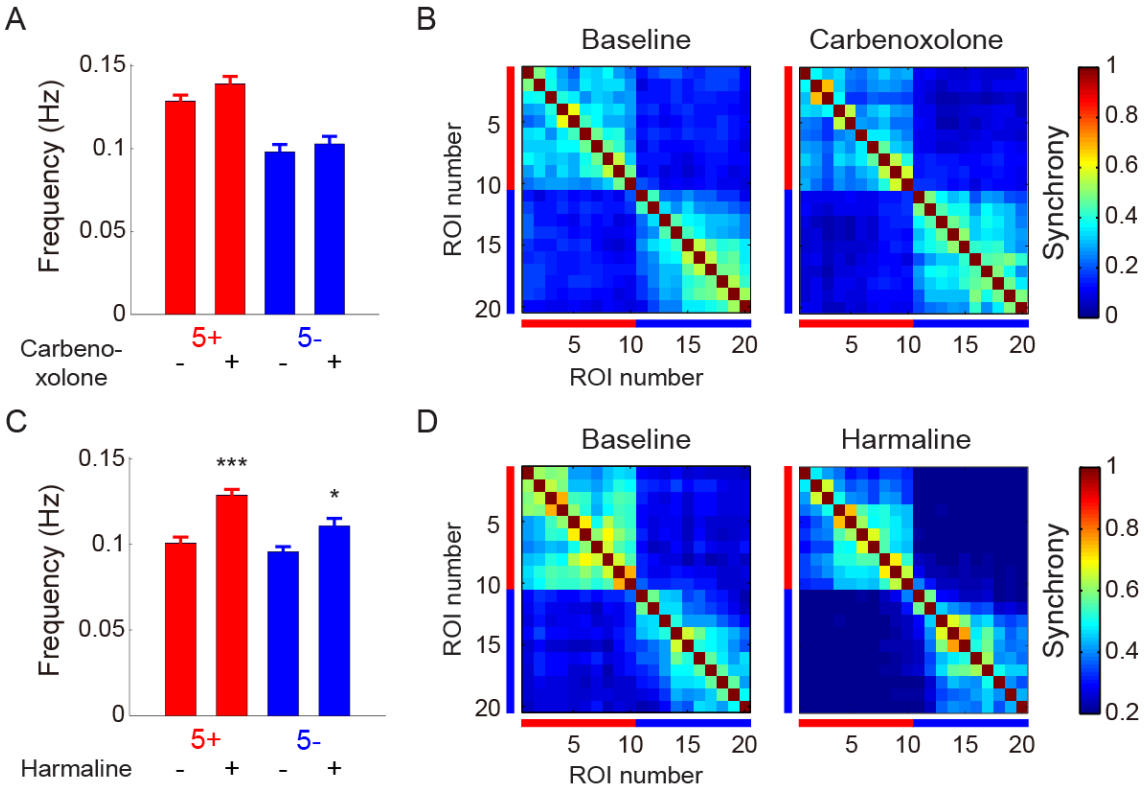


**Figure 5.**

Relationship between aldolase C compartments and complex spike synchrony remains unchanged after pharmacological interventions.

***A***, Averaged frequency of calcium transient in PCs within aldolase C-positive (red) and -negative (blue) compartments before and after carbenoxolone application (baseline: 49 and 44 cells, carbenoxolone: 52 and 41 cells for 5+ and 5- compartment, respectively, *n* = 3 mice). Data are represented as mean ± SEM. No significant difference was observed (Mann Whitney U test). ***B***, Correlation matrices averaged across mice (*n* = 3 mice) before and after carbenoxolone application. Red and blue bars denote aldolase C-positive and -negative PCs, respectively. ***C***, Same as A, but using harmaline (baseline: 46 and 38 cells, harmaline: 50 and 43 cells for 5+ and 5- compartment, respectively, *n* = 3 mice). Data are represented as mean ± SEM. *: $p < 0.05$, ***: $p < 0.001$, Mann Whitney U test. ***D***, Same as B, but using harmaline (*n* = 3 mice). Note that the boundaries of synchrony are unaffected by injections of either carbenoxolone or harmaline.

**Sensory-evoked synchronous complex spike activities are also regulated to be within an aldolase C compartment**

The cerebellar folium Crus IIa of rodents processes tactile sensory information from the perioral region [31]. This folium is therefore a suitable location to investigate the relationships between aldolase C compartments and sensory-evoked complex spike activities. For this purpose, I stimulated the ipsilateral perioral surface using air puffs while performing calcium imaging at the boundaries of aldolase C expression (Fig. 6A and B). Sensory-evoked complex spike responses were observed at particular clusters of PC dendrites, representing classical microzones [3] (Fig. 6C). The responses were most consistently observed at several PCs in the 6- compartment (Fig. 6D). The response profile was sharply delineated at the 7+/6- boundary (Fig. 6D, the left-most panel).

Next, I examined if complex spike responses within this microzone are synchronized in response to the sensory stimulus. I calculated the complex spike synchrony during air puff stimulation and compared it to that of spontaneous events. Correlation matrices during air puff stimulation were averaged across all trials of all mice examined. Correlation matrices of spontaneous events at the same locations were compared with these evoked matrices. As a result, complex spike synchrony was specifically induced within the 6- compartment at the 7+/6- boundary during air puff

stimulation (Fig. 6E). This increase in synchrony was observed at single trial basis (Supplementary Fig. 2). Complex spike synchrony was also induced at other locations but there were no corresponding sensory responses (Fig. 6D, E).

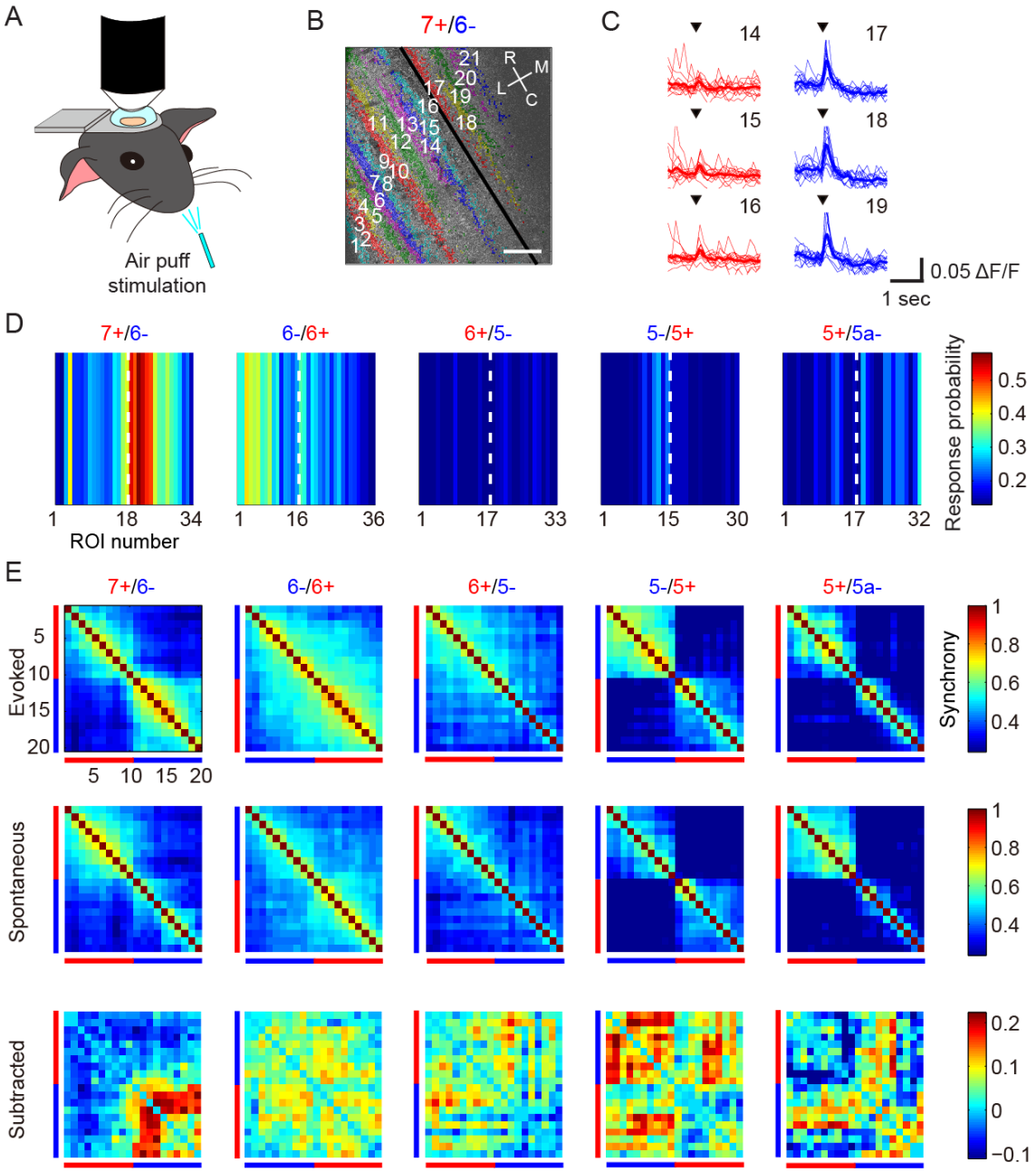


**Figure 6.**

Complex spike synchrony is specifically enhanced at sensory-evoked microzone.

***A***, Schematic experimental settings. Mice received air puff stimulation during calcium imaging. ***B***, Representative tdTomato image at 7+/6- boundary where sensory response was consistently observed. Pseudo-colored PC dendrites are overlaid. Black line represents the 7+/6- aldolase C boundary. R: rostral, C: caudal, L: lateral, and M: medial. Scale bar, 40 μm. ***C***, Sensory-evoked calcium transients around the 7+/6- boundary in B. Thick lines represent the average of responses in one imaging session (13 trials). Black

inverted triangles denote the onset of air puff stimuli. ***D***, Color-coded response probability of PCs near aldolase C boundaries in left Crus II. White broken lines represent aldolase C boundaries. The numbers of regions of interest proximal to the aldolase C boundaries are shown for clarity. *n* = 7, 7, 8, 5, and 3 mice at the 7+/6-, 6-/6+, 6+/5-, 5-/5+, and 5+/5a- compartments, respectively. ***E***, Correlation matrices during air puff trials (top row) compared to that of the spontaneous events during the same period (middle row). Matrices in the bottom row were generated by subtracting the spontaneous matrices from the evoked ones. Red and blue bars represent PC dendrites in aldolase C-positive and -negative compartments, respectively. *n* = 6, 7, 8, 5, and 3 mice for the 7+/6-, 6-/6+, 6+/5-, 5-/5+, and 5+/5a- compartments, respectively.

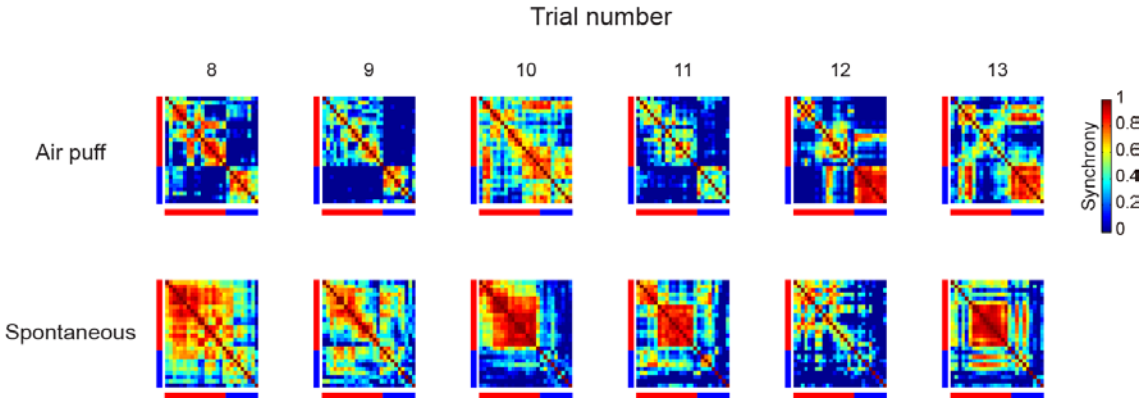


**Supplementary Figure 2.**

Complex spike synchrony within microzone is induced by single air puff.

Correlation matrices at the aldolase C expression boundary (7+/6-) during air puff stimulation in one imaging session (upper row) and corresponding spontaneous matrices (lower row) in the same animal. Data from the last 6 trials of 13 trials are shown. Red and blue bars represent the aldolase C-positive and -negative PCs, respectively. Note that single stimulus can induce complex spike synchrony at sensory microzone in the 6-compartment (8, 9, 11-13).

**Co-activation of microzones across aldolase C compartments in awake mice**

Next, I examined if synchronous complex spike activities during sensory stimulation are dependent on vigilance state. Mice were acclimated to head fixation before experiments and temporarily woken after imaging under anesthesia when they received air puff stimuli. During awake state, the sensory response rate was increased and response profile was extended beyond the boundary of aldolase C compartments (7+/6- boundary; Fig. 7A). Then, I examined whether complex spike synchrony was also modulated during awake state. The correlation matrix obtained during air puff stimulation in awake mice revealed highly synchronous complex spike activities across the 7+/6- boundary (Fig. 7B, right), in a way that two neighboring microzones located in different aldolase C compartments were co-activated (areas a and d in Fig. 7C left). In fact, synchrony both within and between these microzones were significantly increased in awake animals (areas a/d and b, respectively, Fig. 7C right).

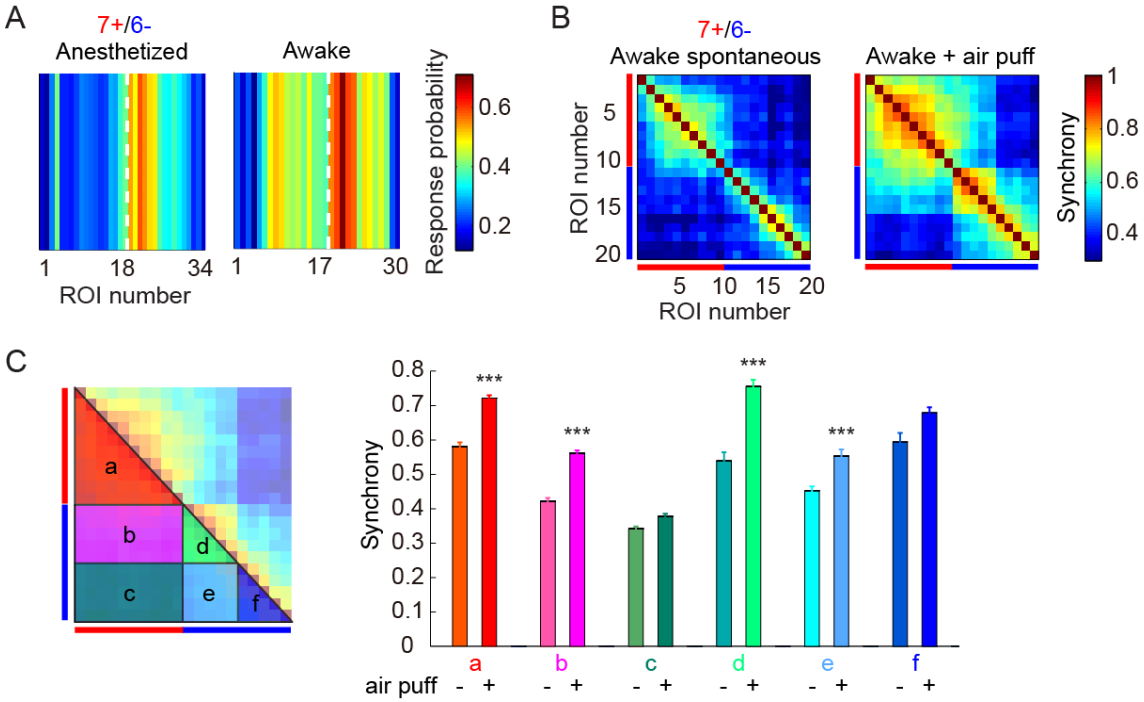


**Figure 7.**

Microzones are co-activated during sensory stimulation in awake mice.

***A***, Left, color-coded response probability of PCs around the 7+/6- aldolase C boundary in Crus II (same data as Fig. 6D, left most panel). Right, same as the left panel, but during awake state. White broken lines represent the aldolase C boundary. *n* = 6 and 3 mice for anesthetized and awake states, respectively. ***B***, Correlation matrices of calcium transients in PCs at the 7+/6- boundary in awake mice during periods with (right) and without (left) air puff stimulation. Red and blue bars represent dendrites in aldolase C-positive and -negative compartments, respectively. *n* = 3 mice. ***C***, Right, averaged complex spike synchrony calculated using matrices in B within areas depicted on the left (a-f), without (-) and with (+) air puff stimulation. Data are represented as mean ± SEM. ***: $p < 0.001$, two-way ANOVA followed by post-hoc Tukey test.

## DISCUSSION

I performed two-photon calcium imaging using knock-in mice (Aldoc-tdTomato mice) in which aldolase C compartments are visualized *in vivo*. I found that complex spikes were significantly synchronized within aldolase C compartments but not across the compartments at single cell resolution. The synchrony depends on medio-lateral distance between PCs within the compartments and several highly synchronous structures existed within single compartments. A sensory-evoked microzone was located in line with aldolase C compartments and sensory-evoked complex spike activities were synchronized within the microzone. I also found that different microzones could be co-activated across aldolase C compartments during sensory stimulation in awake animals.

### Aldoc-tdTomato mouse line as a powerful tool for investigating structure-function relationships of the cerebellar cortex

Aldoc-tdTomato mouse enables us to visualize the longitudinal zones characterized by the aldolase C expression *in vivo* (Fig. 1). Aldoc-tdTomato mouse line has great advantages for the functional analysis of cerebellar cortex, because they enable us to identify aldolase C-positive and -negative PCs *in vivo* and to make targeted imaging or

recordings from these cells in an intact cerebellum. Notably, this mouse line allows us to monitor activities of PCs precisely in the same location across different animals. Furthermore, since I used a “red” fluorescent protein, tdTomato, to visualize aldolase C-positive PCs, “green” functional probes such as GCaMPs can be easily used in the same mice. The use of aldolase C as a marker for the zones also facilitates manipulation (e.g., optogenetics) of cerebellar functions related to motor coordination and learning [32].

**Functional differences between aldolase C-positive and -negative PCs**

A previous electrophysiological study using awake wild type animals showed that firing properties are different between aldolase C-positive and -negative PCs [33]. I found that the frequency of complex spikes tended to be higher and that of simple spikes tended to be lower in aldolase C-positive PCs in Crus II (Fig. 2 and Table 1), which was consistent with the previous study [33]. I could also observe significant differences in complex spike regularity, length of complex spike-induced simple spike pauses, and the number of spikelets in each complex spike (Fig.2 and Table 1). The function of aldolase C molecule in the cerebellum is still largely unclear. At least, I could not observe any knock-in effect, although aldolase C expression level might be lower in the

Aldoc-tdTomato mice. However, other physiologically important molecules (e.g., metabotropic glutamate receptor mGluR1b, phospholipase Cβ3/4, protein kinase Cδ and glutamate transporter EAAT4) in PCs are known to exhibit the same or complementary stripe-shaped expression patterns as aldolase C [18, 34-36]. Therefore, the difference in firing properties may reflect the difference in excitability of PCs and information processing between aldolase C-positive and -negative compartments.

**Aldolase C compartments are consisted of several functional microzones**

The longitudinal zones/microzones were originally defined by the differential axonal projections to cerebellar nuclei and differential climbing fiber inputs from the inferior olivary subnuclei [1, 2]. On the other hand, recent studies using two-photon microscopy have found spatially fine longitudinal structures with high medio-lateral complex spike synchrony. These structures are also thought as microzones [11, 13]. However, they lack anatomical basis to probe cellular relationships between the classically defined zones/microzones and functional complex spike synchrony.

In the present study, I combined genetics and fine scale imaging to elucidate the cell-level precise relationships between complex spike synchrony and anatomically defined zones. I found that spontaneous complex spike activities were significantly

synchronized within the aldolase C compartments, and the synchrony was sharply demarcated at the boundaries of aldolase C expression at single cell resolution (Fig. 4A-B). These results give us the first evidence that fine scale complex spike synchrony is conformed to the zones represented by aldolase C expression.

Next question is whether zones represent homogenously synchronous structures or they are consisted of several fine scale synchronous structures. Previous studies have shown that several clusters of PCs with high complex spike synchrony whose widths are up to 100 μm are aligned medio-laterally [12-14]. Considering that widths of aldolase C compartments are 300-400 μm, there might be several high synchrony areas within the aldolase C compartments. My statistical results showed that complex spike synchrony between medio-laterally closely located PCs were significantly higher within the aldolase C compartments, while the synchrony between distant (>100 μm) PCs was almost the same between within and across the aldolase C compartments (Fig. 4C). Moreover, I found more than one high synchrony areas within a single aldolase C compartment (Fig. 4E). These results indicate that the zones represented by aldolase C expression are consisted of several functional microzones in which complex spikes are highly synchronized.

**Mechanism of the delineation of complex spike synchrony at the boundaries of aldolase C expression**

To address why complex spike synchrony is finely delineated at the boundaries of aldolase C expression, I pharmacologically blocked electrical couplings between inferior olivary neurons using carbenoxolone or excite these neurons using harmaline. However, neither carbenoxolone nor harmaline affected the boundaries of complex spike synchrony in reference to those of aldolase C expression (Fig. 5). These results suggest that climbing fiber projection itself defines the boundaries of fine scale complex spike synchrony; different populations of inferior olivary neurons precisely project to PCs in each aldolase C compartment, although I cannot exclude the possibility that treatment with carbenoxolone did not sufficiently block electrical couplings. I also found the aldolase C boundaries which did not show clear correspondence to complex spike synchrony (Fig. 4; 6-/6+ and 6+/5-). At these boundaries, gap junctions might be formed beyond the boundaries of inferior olivary subnuclei as reported previously [20].

**Establishment of precise correlation between the aldolase C compartments and complex spike synchrony**

Formation of aldolase C compartments is developmentally regulated. Mediolateral

compartmentalization of PCs is dependent on birth date [16] and is closely correlated with the longitudinal stripes of aldolase C expression [37]. Projection of climbing fibers to PCs is also developmentally regulated. Morphological reconstruction of single climbing fibers in P4-7 rats has revealed that nascent climbing fibers project to PCs aligned with parasagittally oriented narrow bands [38]. Therefore, the overall relationship between aldolase C compartments and climbing fiber innervation may already be determined at the neonatal stage by axon guidance based on molecular recognition. On the other hand, one-to-one climbing fiber to PC connectivity is established by strengthening single climbing fibers and eliminating redundant ones during the early postnatal period, in an activity-dependent manner [39, 40]. This activity-dependent climbing fiber elimination process [41, 42] presumably plays a role in fine tuning the precise relationship between aldolase C compartments and complex spike synchrony.

**Functional complex spike synchrony in microzones**

Even within a microzone, complex spike synchrony was not homogenous, but significantly attenuated in the medio-lateral direction (Fig. 4C). This medio-lateral attenuation of synchrony might be maintained by moderate level of electrical couplings

between inferior olivary neurons [10] that project to the microzone, although my pharmacological experiment using carbenoxolone could not add clear evidence to this. This graded synchrony in the medio-lateral direction might make a room for enhancing synchrony within a microzone in need. In fact, previous studies suggest that complex spike synchrony can be induced within microzones during sensorimotor activities [11, 13]. I also addressed this enhancement of synchrony within microzones by sensory stimulation. A microzone was located at the lateral boundary of 6- compartment using targeted perioral sensory stimulus (Fig. 6D). Complex spike synchrony was specifically induced in this microzone by sensory stimulation (Fig. 6E). This increase was observed in single trials (Supplementary Fig. 2). These results indicate that microzones function by synchronizing complex spike activities [11]. Synchronous complex spike activities in large number of PCs cause strong inhibition and subsequent rebound firing in the cerebellar nuclear neurons, which is important for cerebellum-dependent motor coordination and learning [43]. Therefore, at spontaneous state, complex spikes are not necessarily synchronized in microzones, but they are synchronized as necessary during sensory processing. On the other hand, complex spike synchrony is also known to be weakly attenuated in the rostro-caudal direction [6]. In my two-photon imaging setting, however, fine scale synchrony along a broad range of rostro-caudal axis of microzone

could not be examined. Macroscopic calcium imaging with fine spatial resolution will elucidate whether PCs synchronize all along the entire microzones during functioning.

**Different microzones cooperate during awake state**

I found that microzones were consistently co-activated across aldolase C boundaries during sensory stimulation in awake mice (7+/6- boundary; Fig. 7B). Microzone at 7+ was only activated during awake state when sensory-evoked motor responses were observed. Moreover, extensive projections are known to exist from motor and association areas of the cerebral cortex to the lateral cerebellum [44], the region which I examined in the present study. It is therefore possible that the microzone at 7+ is involved in motor or cognitive functions. Co-activation of neighboring microzones implies the facilitation of coupling between microzones with different (e.g., sensory and motor) modalities under awake conditions. Presumed weak coupling between tightly coupled cell assemblies in the inferior olive might be enhanced, leading to the elevation of synchrony between these assemblies during awake condition [45]. This flexible coordination of microzones may further facilitate cerebellum-dependent sensorimotor processing and learning. Application of highly efficient motor tasks [46, 47] will further elucidate the relationship between coordinated microzonal activities and sensorimotor

functions.

**Simple and complex spike outputs from zones/microzones**

The limitation of my study is that only complex spikes of PCs can be monitored with calcium imaging. PCs *in vivo* show ongoing simple spike activities at 50-100 Hz, which could be modified by parallel fiber inputs and inhibitory inputs from molecular layer interneurons. Complex spikes are known to have significant influence on simple spike activities [48-51]. Climbing fiber inputs induce simple spike pause through molecular layer interneurons [52] and calcium dependent potassium channels on PC membrane [53]. Simple spike pauses in individual PCs may have negligible effects on firing of deep cerebellar nuclear neurons that project to various regions of the brain to modify motor and cognitive processes [54]. However, simple spike pauses may be able to significantly influence the firings of deep cerebellar nuclear neurons when the pauses are synchronized in large number of PCs. Indeed, it has been shown that simple spike synchrony induces transient inhibition and subsequent rebound firing of deep cerebellar nuclear neurons [55]. Therefore, it is important to elucidate whether simple spikes and simple spike pause of PCs in the same aldolase C compartment are synchronized or not. Visually-guided multiunit recordings or voltage imaging using fluorogenic voltage

sensor proteins [56] in Aldoc-tdTomato mice will address this issue. In addition to synchronized simple spikes, synchronous complex spikes in large number of PCs also results in rebound firing of deep cerebellar nuclear neurons [43]. However, how synchronous complex spike and simple spike inputs converge on deep cerebellar nuclear neurons and how these inputs are encoded in these cells remain largely unknown. Simultaneous imaging of complex spike and simple spike activities in population of PCs in conjunction with targeted recording from cerebellar nuclear neurons in behaving Aldoc-tdTomato mice will be required to further elucidate the spatiotemporal information processing in the cerebellar zones/microzones.

**ACKNOWLEDGEMENTS**

I would like to express my sincere gratitude to Professor Masanobu Kano for supervision during my Ph-D course. I am also grateful to Professor Kazuo Kitamura for warm instruction of experiments and for fruitful discussion. I also thank M. Hashizume for technical assistance, M. Tada for participation in preliminary experiments, T. Ishikawa for providing analysis software (TaroTools for Igor Pro), T. Kawashima for advice on Matlab routines, Simon Schultz, Masanori Matsuzaki, Yoshikazu Isomura and members of Kano lab for discussion. Finally, I specially thank Dr. Taisuke Miyazaki and Professor Masahiko Watanabe for morphological analysis and Dr. Maya Yamazaki and Professor Kenji Sakimura for generating Aldoc-tdTomato knock-in mice.

## REFERENCES


1. Groenewegen, H.J., J. Voogd, and S.L. Freedman, *The parasagittal zonation within the olivocerebellar projection. II. Climbing fiber distribution in the intermediate and hemispheric parts of cat cerebellum.* J Comp Neurol, 1979. **183**(3): p. 551-601.
2. Voogd, J. and M. Glickstein, *The anatomy of the cerebellum.* Trends Neurosci, 1998. **21**(9): p. 370-5.
3. Andersson, G. and O. Oscarsson, *Climbing fiber microzones in cerebellar vermis and their projection to different groups of cells in the lateral vestibular nucleus.* Exp Brain Res, 1978. **32**(4): p. 565-79.
4. Oscarsson, O., *Functional Units of the Cerebellum - Sagittal Zones and Microzones.* Trends Neurosci, 1979. **2**(6): p. 143-145.
5. Apps, R. and M. Garwicz, *Anatomical and physiological foundations of cerebellar information processing.* Nat Rev Neurosci, 2005. **6**(4): p. 297-311.
6. Bell, C.C. and T. Kawasaki, *Relations among climbing fiber responses of nearby Purkinje Cells.* J Neurophysiol, 1972. **35**(2): p. 155-69.
7. Sasaki, K., J.M. Bower, and R. Llinas, *Multiple Purkinje Cell Recording in Rodent Cerebellar Cortex.* Eur J Neurosci, 1989. **1**(6): p. 572-586.
8. Sugihara, I., H.S. Wu, and Y. Shinoda, *The entire trajectories of single olivocerebellar axons in the cerebellar cortex and their contribution to Cerebellar compartmentalization.* J Neurosci, 2001. **21**(19): p. 7715-23.
9. Voogd, J., J. Pardoe, T.J. Ruigrok, and R. Apps, *The distribution of climbing and mossy fiber collateral branches from the copula pyramidis and the paramedian lobule: congruence of climbing fiber cortical zones and the pattern of zebrin banding within the rat cerebellum.* J Neurosci, 2003. **23**(11): p. 4645-56.
10. Blenkinsop, T.A. and E.J. Lang, *Block of inferior olive gap junctional coupling decreases Purkinje cell complex spike synchrony and rhythmicity.* J Neurosci, 2006. **26**(6): p. 1739-48.
11. Schultz, S.R., K. Kitamura, A. Post-Uiterweer, J. Krupic, and M. Hausser, *Spatial pattern coding of sensory information by climbing fiber-evoked calcium signals in networks of neighboring cerebellar Purkinje cells.* J Neurosci, 2009. **29**(25): p. 8005-15.
12. Ozden, I., M.R. Sullivan, H.M. Lee, and S.S. Wang, *Reliable coding emerges from coactivation of climbing fibers in microbands of cerebellar Purkinje neurons.* J Neurosci, 2009. **29**(34): p. 10463-73.

13. Mukamel, E.A., A. Nimmerjahn, and M.J. Schnitzer, *Automated analysis of cellular signals from large-scale calcium imaging data.* Neuron, 2009. **63**(6): p. 747-60.
14. Ghosh, K.K., L.D. Burns, E.D. Cocker, A. Nimmerjahn, Y. Ziv, A.E. Gamal, and M.J. Schnitzer, *Miniaturized integration of a fluorescence microscope.* Nat Methods, 2011. **8**(10): p. 871-8.
15. Brochu, G., L. Maler, and R. Hawkes, *Zebrin II: a polypeptide antigen expressed selectively by Purkinje cells reveals compartments in rat and fish cerebellum.* J Comp Neurol, 1990. **291**(4): p. 538-52.
16. Hashimoto, M. and K. Mikoshiba, *Mediolateral compartmentalization of the cerebellum is determined on the "birth date" of Purkinje cells.* J Neurosci, 2003. **23**(36): p. 11342-51.
17. Oberdick, J., S.L. Baader, and K. Schilling, *From zebra stripes to postal zones: deciphering patterns of gene expression in the cerebellum.* Trends Neurosci, 1998. **21**(9): p. 383-90.
18. Sarna, J.R., H. Marzban, M. Watanabe, and R. Hawkes, *Complementary stripes of phospholipase Cβ3 and Cβ4 expression by Purkinje cell subsets in the mouse cerebellum.* J Comp Neurol, 2006. **496**(3): p. 303-13.
19. Sugihara, I. and P.N. Quy, *Identification of aldolase C compartments in the mouse cerebellar cortex by olivocerebellar labeling.* J Comp Neurol, 2007. **500**(6): p. 1076-92.
20. Sugihara, I., S.P. Marshall, and E.J. Lang, *Relationship of complex spike synchrony bands and climbing fiber projection determined by reference to aldolase C compartments in crus IIa of the rat cerebellar cortex.* J Comp Neurol, 2007. **501**(1): p. 13-29.
21. Mishina, M. and K. Sakimura, *Conditional gene targeting on the pure C57BL/6 genetic background.* Neurosci Res, 2007. **58**(2): p. 105-12.
22. Fujita, H., H. Aoki, I. Ajioka, M. Yamazaki, M. Abe, A. Oh-Nishi, K. Sakimura, and I. Sugihara, *Detailed expression pattern of aldolase C (Aldoc) in the cerebellum, retina and other areas of the CNS studied in Aldoc-Venus knock-in mice.* PLoS One, 2014. **9**(1): p. e86679.
23. Pologruto, T.A., B.L. Sabatini, and K. Svoboda, *ScanImage: flexible software for operating laser scanning microscopes.* Biomed Eng Online, 2003. **2**: p. 13.
24. Hashizume, M., T. Miyazaki, K. Sakimura, M. Watanabe, K. Kitamura, and M. Kano, *Disruption of cerebellar microzonal organization in GluD2 (GluRδ2) knockout mouse.* Front Neural Circuits, 2013. **7**: p. 130.

25. Tada, M., A. Takeuchi, M. Hashizume, K. Kitamura, and M. Kano, *A highly sensitive fluorescent indicator dye for calcium imaging of neural activity in vitro and in vivo.* Eur J Neurosci, 2014. **39**(11): p. 1720-8.
26. Kitamura, K., B. Judkewitz, M. Kano, W. Denk, and M. Hausser, *Targeted patch-clamp recordings and single-cell electroporation of unlabeled neurons in vivo.* Nat Methods, 2008. **5**(1): p. 61-7.
27. Ozden, I., H.M. Lee, M.R. Sullivan, and S.S. Wang, *Identification and clustering of event patterns from in vivo multiphoton optical recordings of neuronal ensembles.* J Neurophysiol, 2008. **100**(1): p. 495-503.
28. Smith, S.L. and M. Hausser, *Parallel processing of visual space by neighboring neurons in mouse visual cortex.* Nat Neurosci, 2010. **13**(9): p. 1144-9.
29. Kitamura, K. and M. Hausser, *Dendritic calcium signaling triggered by spontaneous and sensory-evoked climbing fiber input to cerebellar Purkinje cells in vivo.* J Neurosci, 2011. **31**(30): p. 10847-58.
30. Miwa, H., *Rodent models of tremor.* Cerebellum, 2007. **6**(1): p. 66-72.
31. Brown, I.E. and J.M. Bower, *Congruence of mossy fiber and climbing fiber tactile projections in the lateral hemispheres of the rat cerebellum.* J Comp Neurol, 2001. **429**(1): p. 59-70.
32. Tsubota, T., Y. Ohashi, and K. Tamura, *Optogenetics in the cerebellum: Purkinje cell-specific approaches for understanding local cerebellar functions.* Behav Brain Res, 2013. **255**: p. 26-34.
33. Zhou, H., Z. Lin, K. Voges, C. Ju, Z. Gao, L.W. Bosman, T.J. Ruigrok, F.E. Hoebeek, C.I. De Zeeuw, and M. Schonewille, *Cerebellar modules operate at different frequencies.* Elife, 2014: p. e02536.
34. Paukert, M., Y.H. Huang, K. Tanaka, J.D. Rothstein, and D.E. Bergles, *Zones of enhanced glutamate release from climbing fibers in the mammalian cerebellum.* J Neurosci, 2010. **30**(21): p. 7290-9.
35. Wang, X., G. Chen, W. Gao, and T.J. Ebner, *Parasagittally aligned, mGluR1-dependent patches are evoked at long latencies by parallel fiber stimulation in the mouse cerebellar cortex in vivo.* J Neurophysiol, 2011. **105**(4): p. 1732-46.
36. Chen, S. and D.E. Hillman, *Compartmentation of the cerebellar cortex by protein kinase C delta.* Neuroscience, 1993. **56**(1): p. 177-88.
37. Namba, K., I. Sugihara, and M. Hashimoto, *Close correlation between the birth date of Purkinje cells and the longitudinal compartmentalization of the mouse adult cerebellum.* J Comp Neurol, 2011. **519**(13): p. 2594-614.

38. Sugihara, I., *Microzonal projection and climbing fiber remodeling in single olivocerebellar axons of newborn rats at postnatal days 4-7.* J Comp Neurol, 2005. **487**(1): p. 93-106.
39. Hashimoto, K. and M. Kano, *Functional differentiation of multiple climbing fiber inputs during synapse elimination in the developing cerebellum.* Neuron, 2003. **38**(5): p. 785-96.
40. Hashimoto, K., M. Tsujita, T. Miyazaki, K. Kitamura, M. Yamazaki, H.S. Shin, M. Watanabe, K. Sakimura, and M. Kano, *Postsynaptic P/Q-type $Ca^{2+}$ channel in Purkinje cell mediates synaptic competition and elimination in developing cerebellum.* Proc Natl Acad Sci U S A, 2011. **108**(24): p. 9987-92.
41. Mikuni, T., N. Uesaka, H. Okuno, H. Hirai, K. Deisseroth, H. Bito, and M. Kano, *Arc/Arg3.1 is a postsynaptic mediator of activity-dependent synapse elimination in the developing cerebellum.* Neuron, 2013. **78**(6): p. 1024-35.
42. Fukaya, M., M. Tsujita, M. Yamazaki, E. Kushiya, M. Abe, K. Akashi, R. Natsume, M. Kano, H. Kamiya, M. Watanabe, and K. Sakimura, *Abundant distribution of TARP gamma-8 in synaptic and extrasynaptic surface of hippocampal neurons and its major role in AMPA receptor expression on spines and dendrites.* Eur J Neurosci, 2006. **24**(8): p. 2177-90.
43. Bengtsson, F., C.F. Ekerot, and H. Jorntell, *In vivo analysis of inhibitory synaptic inputs and rebounds in deep cerebellar nuclear neurons.* PLoS One, 2011. **6**(4): p. e18822.
44. Sasaki, K., H. Oka, Y. Matsuda, T. Shimono, and N. Mizuno, *Electrophysiological studies of the projections from the parietal association area to the cerebellar cortex.* Exp Brain Res, 1975. **23**(1): p. 91-102.
45. De Zeeuw, C.I., F.E. Hoebeek, L.W. Bosman, M. Schonewille, L. Witter, and S.K. Koekkoek, *Spatiotemporal firing patterns in the cerebellum.* Nat Rev Neurosci, 2011. **12**(6): p. 327-44.
46. Isomura, Y., R. Harukuni, T. Takekawa, H. Aizawa, and T. Fukai, *Microcircuitry coordination of cortical motor information in self-initiation of voluntary movements.* Nat Neurosci, 2009. **12**(12): p. 1586-93.
47. Hira, R., F. Ohkubo, K. Ozawa, Y. Isomura, K. Kitamura, M. Kano, H. Kasai, and M. Matsuzaki, *Spatiotemporal dynamics of functional clusters of neurons in the mouse motor cortex during a voluntary movement.* J Neurosci, 2013. **33**(4): p. 1377-90.
48. Cerminara, N.L. and J.A. Rawson, *Evidence that climbing fibers control an intrinsic spike generator in cerebellar Purkinje cells.* J Neurosci, 2004. **24**(19): p.

4510-7.
49. Ebner, T.J. and J.R. Bloedel, *Temporal patterning in simple spike discharge of Purkinje cells and its relationship to climbing fiber activity.* J Neurophysiol, 1981. **45**(5): p. 933-47.
50. Granit, R. and C.G. Phillips, *Excitatory and inhibitory processes acting upon individual Purkinje cells of the cerebellum in cats.* J Physiol, 1956. **133**(3): p. 520-47.
51. Loewenstein, Y., S. Mahon, P. Chadderton, K. Kitamura, H. Sompolinsky, Y. Yarom, and M. Hausser, *Bistability of cerebellar Purkinje cells modulated by sensory stimulation.* Nat Neurosci, 2005. **8**(2): p. 202-11.
52. Mathews, P.J., K.H. Lee, Z. Peng, C.R. Houser, and T.S. Otis, *Effects of climbing fiber driven inhibition on Purkinje neuron spiking.* J Neurosci, 2012. **32**(50): p. 17988-97.
53. McKay, B.E., J.D. Engbers, W.H. Mehaffey, G.R. Gordon, M.L. Molineux, J.S. Bains, and R.W. Turner, *Climbing fiber discharge regulates cerebellar functions by controlling the intrinsic characteristics of purkinje cell output.* J Neurophysiol, 2007. **97**(4): p. 2590-604.
54. Lu, X., S. Miyachi, and M. Takada, *Anatomical evidence for the involvement of medial cerebellar output from the interpositus nuclei in cognitive functions.* Proc Natl Acad Sci U S A, 2012. **109**(46): p. 18980-4.
55. Person, A.L. and I.M. Raman, *Purkinje neuron synchrony elicits time-locked spiking in the cerebellar nuclei.* Nature, 2012. **481**(7382): p. 502-5.
56. Jin, L., Z. Han, J. Platisa, J.R. Wooltorton, L.B. Cohen, and V.A. Pieribone, *Single action potentials and subthreshold electrical events imaged in neurons with a fluorescent protein voltage probe.* Neuron, 2012. **75**(5): p. 779-85.

Part of this work was published as an original paper;

Shinichiro Tsutsumi, Maya Yamazaki, Taisuke Miyazaki, Masahiko Watanabe, Kenji Sakimura, Masanobu Kano, and Kazuo Kitamura: Structure-Function Relationships between Aldolase C/Zebrin II Expression and Complex Spike Synchrony in the Cerebellum. J Neurosci 35, 843–852 (2015).